Network Analysis of European Winter Temperatures and their Relationship to the Quasi-Biennial Oscillation

David Strahl[1]

[1]Universität Potsdam

Correspondence: david.strahl@uni-potsdam.de

Abstract. Complex network theory has been shown to be a powerful tool for revealing patterns and drivers of natural climate variability, leading to a better understanding of climate change in general. In the past, global climate networks have been constructed from temperature data in combination with correlation measures like the linear Pearson correlation or the non-linear Mutual Information. Novel methods based on phase space recurrences have equally been proposed in this context, however it is unclear whether they perform reliably for gridded data. This study evaluates the efficacy of using recurrence-based networks to detect the influence of the quasi-biennial oscillation (QBO) on European winter temperatures and compares their performance to traditional Pearson networks. It was found that recurrence-based networks show similar overall properties to Pearson networks, but exhibit differences on the local scale due to their ability to capture non-linear relationships. It was not possible to detect a significant effect of the QBO on European winter temperatures, but this is mainly attributed to limitations in the study's design rather than the method's applicability in general. Results suggest that with increased computational power, effects of the QBO could be unveiled. In the broader context, this study illustrates why further work on complex climate networks will be necessary to develop a thorough methodological framework and increase confidence in the derived results.

1 Introduction

The quasi-biennial oscillation (QBO) is a large scale atmospheric oscillation pattern of the mean zonal wind in the equatorial stratosphere. Winds change quasi-periodically between a westerly and easterly phase, with a period of roughly 28 months (Baldwin et al., 2001) The easterly phase is on average twice as strong and sustained longer at higher altitudes, while the reverse is true for the westerly phase (Baldwin et al., 2001). This results in a downward propagation of the QBO. The oscillation is driven by interactions of the mean zonal stratospheric flow with gravity waves emitted from the troposphere (Baldwin et al., 2001).

It has been shown that the QBO has an impact on European winter temperatures. When in an easterly phase during the northern winter, the QBO tends to lead to colder than average temperatures. This is because easterlies strengthen the polar vortex that pushes cold air from the Arctic towards Europe (Baldwin et al., 2001). Conversely, the polar vortex is weakened in the westerly phase allowing warmer air from the tropics to reach Europe, leading to milder than average temperatures.

It has been shown, that complex network theory is a promising tool for finding patterns and teleconnections between elements of the climate system (Donges et al., 2009). Previously, climate networks have been constructed from gridded data using the

Pearson correlation coefficient and the non-linear Mutual Information (Donges et al., 2009). Furthermore, recurrence based correlation measures have been applied to quantify the connections of various components of the climate system with global mean temperature (Goswami et al., 2013).

This report tries to detect the impact of the QBO on European winter temperatures by constructing complex climate networks from correlations in gridded temperature data over Europe. It determines whether static complex networks can at all be constructed from joint recurrence measures and how they compare to ones derived from the linear Pearson correlation. Furthermore, it explores how network properties evolve with time and whether they show continuous or abrupt shifts.

2 Methods

2.1 Data Preparation

For this report I used ERA5 gridded reanalysis data of European mean temperatures. Grid cells are $0.25\,°\times0.25\,°$ and cover an area from $25\,°\mathrm{N}$ to $75\,°\mathrm{N}$ and $35\,°\mathrm{W}$ to $45\,°\mathrm{E}$. All time series cover the years 1981 - 2020 with daily resolution.

Due to the high computational effort that would be needed to construct a complex network from this grid, I decided to coarsen it drastically. I reduced both latitude and longitude resolution by a factor of eight, resulting in an averaged grid of 25×40 cells with a resolution of $2\,°\times2\,°$. Because the original grid size was not perfectly divisible by eight I implicitly discarded a narrow region along its edges.

To further improve computational performance and because this report is only interested in winter temperatures, I filtered the time series to contain only the months October to March (inclusive) and binned it over weeks. For this I used the week number according to the calendar and not a moving average of seven days, as this would introduce shifts due to the variable length of a month.

Based on the central latitude and longitude of each grid cell, I calculated pairwise great circle distances between their centroids. Again, I used the great circle distance because it was substantially faster to compute compared to a geodesic distances. However, due to the small spatial extent of the region under consideration, errors are negligible.

Finally, I downloaded data on the mean zonal wind speed in the tropical stratosphere to reflect the QBO state. This data was taken from the Freie Universität Berlin. I derived a QBO index by taking the yearly average of the $70\,\mathrm{hPa}$ wind speed.

2.2 Building the Complex Network

To build a complex network from gridded data, one considers each grid-cell as a node within the network. For a grid of 25×40 cells, this gives a total of $N = 1000$ nodes. Each link within the network now represents the dependence of one node on another. Therefore, no self loops are allowed and links are non-directional. Hence, a total of $L = N(N-1)/2$ links can be constructed.

To determine whether a pair of nodes will be connected in the network, one looks at the correlation between time series of the corresponding grid cells. This dependence may either be quantified using the linear Pearson correlation or non-linear measures like the Mutual Information or the recurrence based measure of dependence as introduced by Goswami et al. (2013).

2.2.1 Recurrence Based Measure of Dependence

To calculate the recurrence based measure of dependence between a pair of time series $\boldsymbol{x}$ and $\boldsymbol{y}$ one firstly builds recurrence plots by thresholding the distance between states in phase space,

$$R_{ij}(\boldsymbol{x}) = \theta\left(\|x_i - x_j\| - \epsilon\right) \tag{1}$$

where $\|\cdot\|$ denotes an appropriate norm (here absolute difference), $\theta(\cdot)$ is the Heaviside step function and ϵ the distance threshold. For all recurrence plots I used a recurrence rate of $10\,\%$, meaning that ϵ is selected to yield one tenth of the possible recurrences.

The joint recurrence plot indicates whether recurrences happen in both time series at the same time. It is calculated by multiplying the recurrence plots element-wise:

$$JR_{ij}(\boldsymbol{x}, \boldsymbol{y}) = R_{ij}(\boldsymbol{x}) R_{ij}(\boldsymbol{y}) \tag{2}$$

The column-wise and total recurrence rate are defined as

$$RR_i = \frac{1}{T}\sum_{j}^{T} R_{ij} \quad \text{and} \quad RR = \frac{1}{T}\sum_{i,j}^{T} R_{ij} \tag{3}$$

Similar recurrence rates can be calculated for the joint recurrence plots and are denoted JRR_i and JRR.

Finally, the recurrence based measure of dependence is defined as

$$RMD(\boldsymbol{x}, \boldsymbol{y}) = \frac{1}{T}\sum_{i}^{T} \frac{JRR_i(\boldsymbol{x}, \boldsymbol{y})}{RR_i(\boldsymbol{x}) RR_i(\boldsymbol{y})} \tag{4}$$

which is a non-linear correlation measure based on the joint recurrence of $\boldsymbol{x}$ and $\boldsymbol{y}$. Joint recurrence here means that whenever a state of $\boldsymbol{x}$ recurres at one time, another one does so at the same time for $\boldsymbol{y}$.

2.2.2 Statistical Significance

The constructed network should of course only include correlations that are statistically significant. Donges et al. (2009) and Goswami et al. (2013) described a simple procedure based on twin surrogate time series that can be used to test the statistical significance of a correlation. However, implementing this approach here is too computationally exhaustive.

It has been shown, that climate networks are very similar for low link densities (Donges et al., 2009). This motivates a simple ranking of link significance. Given a link density p I discard the lower $1 - p$ quantile of absolute correlation values and construct links only from the Lp largest values. The absolute value is needed here to capture impacts in both directions. This of course implies the assumption that high correlations are also statistically significant, which is reasonably valid for both Pearson correlation and the RMD. Inline with Donges et al. (2009), I used a value of $p = 0.5\,\%$ for both static and evolving networks.

2.3 Correction for Boundary Effects

Rheinwalt et al. (2012) have shown that for spatially confined networks boundary effects become significant and can lead to false interpretations. This is especially true when networks have a low number of nodes, as is the case here. I therefore did a

boundary effect correction by generating a set of surrogate networks. They are used as a baseline to determine the expected value of certain network metrics.

Surrogate networks are generated in the following way: Given a network whose links are derived from statistically significant correlation coefficients, I calculate the physical node distance d for all links to get a link length histogram $C(d)$. The distances are taken from the distance matrix described in the section on data preparation. The same is done for a hypothetical network in which all nodes are connected to give $C_H(d)$. For each distance, the ratio of links with this length in the real network over possible links in the fully-connected network is treated as the probability of having a link given its length:

$$p(\text{connection}|d) = \frac{C(d)}{C_H(d)} \tag{5}$$

From this, I constructed surrogate networks by connecting nodes at random with the given probability. The surrogate network thus shares both the link density and the link length distribution with the original network. All spatially resolved network metrics are corrected by the average of 200 surrogate networks.

2.4 Network Metrics

To analyze the resulting complex networks it is necessary to summarize them into certain metrics that are easier to interpret.

Given that these metrics are well-established I will refrain from defining them here again. I used NETWORKX to calculate the betweenness, closeness centrality, average path length and clustering coefficient (Hagberg et al., 2008). I however implemented the area weighted connectivity (AWC) and Hamming distance myself, as they are not available in the routine. Analytical definitions are given by Donges et al. (2009) and their implementation is described on the documentation page of NETWORKX.

2.5 Evolving Network Construction

To construct an evolving network representation of European winter temperatures, I split the time series into disjoint one-year windows. Each of them starts with the first week of October and ends with the last week of March in the next year. Because the overall data started in January and ended in December, the first and last window are only half the size.

For each window I constructed two networks as described above, one derived from the Pearson correlation and one from the RMD. This yields two evolving series of 41 networks. For each, I calculated the global clustering coefficient, average path length and overall closeness centrality.

Boundary effects are expected to be constant for all networks, as they only depend on the grid. Time series of network metrics would therefore only be transformed linearly. As I am interested in periodic changes, it is then not necessary to correct for boundary effects.

3 Results

3.1 Comparison for Different Link Densities

Fig. 1 shows a comparison between the static Pearson and RMD network for different link densities.

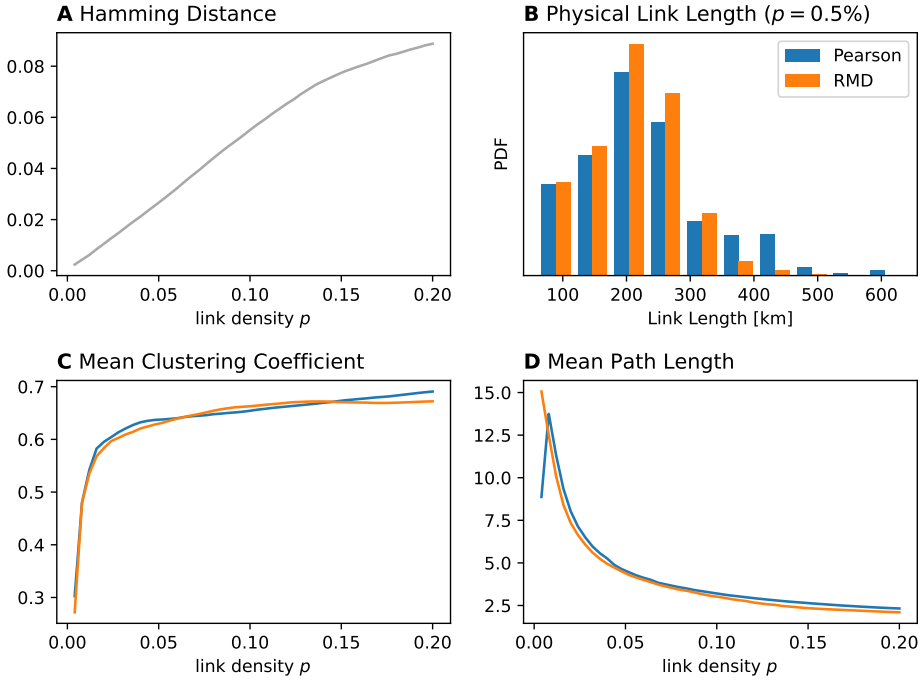

Figure 1. Comparison between Pearson and RMD networks for different link densities. (**A**) Hamming distance between the two networks. (**B**) Physical link length distribution for $p = 0.5\%$. (**C-D**) Mean clustering coefficient and topological path length for different link densities.

The Hamming distance between the two networks (Fig. 1A) falls linearly with link density, indicating that both Pearson and RMD mostly picked up the same correlations in the data. Difference between the two networks of course exist, as can be seen from the physical link length plot (Fig. 1B). The Pearson network slightly favors correlations between nodes that are farther apart. Overall, the link length distribution looks however very similar.

Mean clustering coefficient (Fig. 1C) and mean topological path length (Fig. 1D) are equally similar. For very low link densities a higher mean topological path length is seen for the RMD network. This means, that some links connecting multiple nodes in the Pearson network are not picked up or substituted by a single link for the RMD.

The trend in mean topological path length is similar to the one described by Donges et al. (2009) and indicates that both Pearson and RMD networks exhibit small-world properties. However, for the clustering coefficient an opposite trend is observed here. Clustering is low for small link densities and plateaus for larger densities. A decline with link density, as observed by Donges et al. (2009) is not seen here.

3.2 Area Weighted Connectivity Field

The spatially resolved and boundary-corrected AWC field is shown in Fig. A.1. There are clear differences between the network derived from the Pearson correlation and the one using the RMD.

The Pearson network shows highly connected nodes for lower latitudes that the RMD network does not display. Hubs are mainly located around the Mediterranean and west of Africa. These regions of high degree represent nodes that are highly

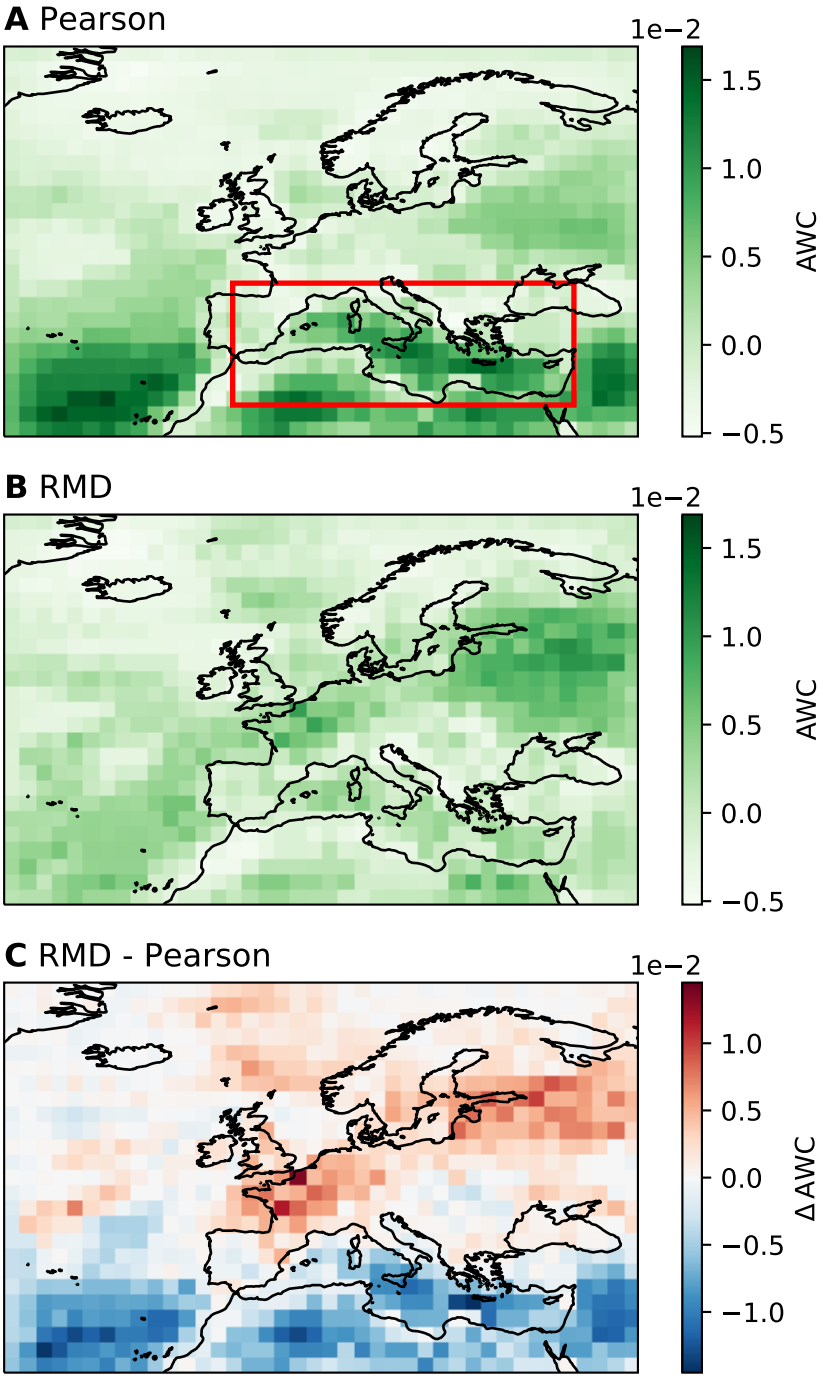

Figure 2. Area weighted connectivity fields for networks derived from Pearson correlation coefficient (**A**), recurrence based measure of dependence (RMD) (**B**) and their difference (**C**). The red inset highlights the Mediterranean for which the evolving network analysis was done separately.

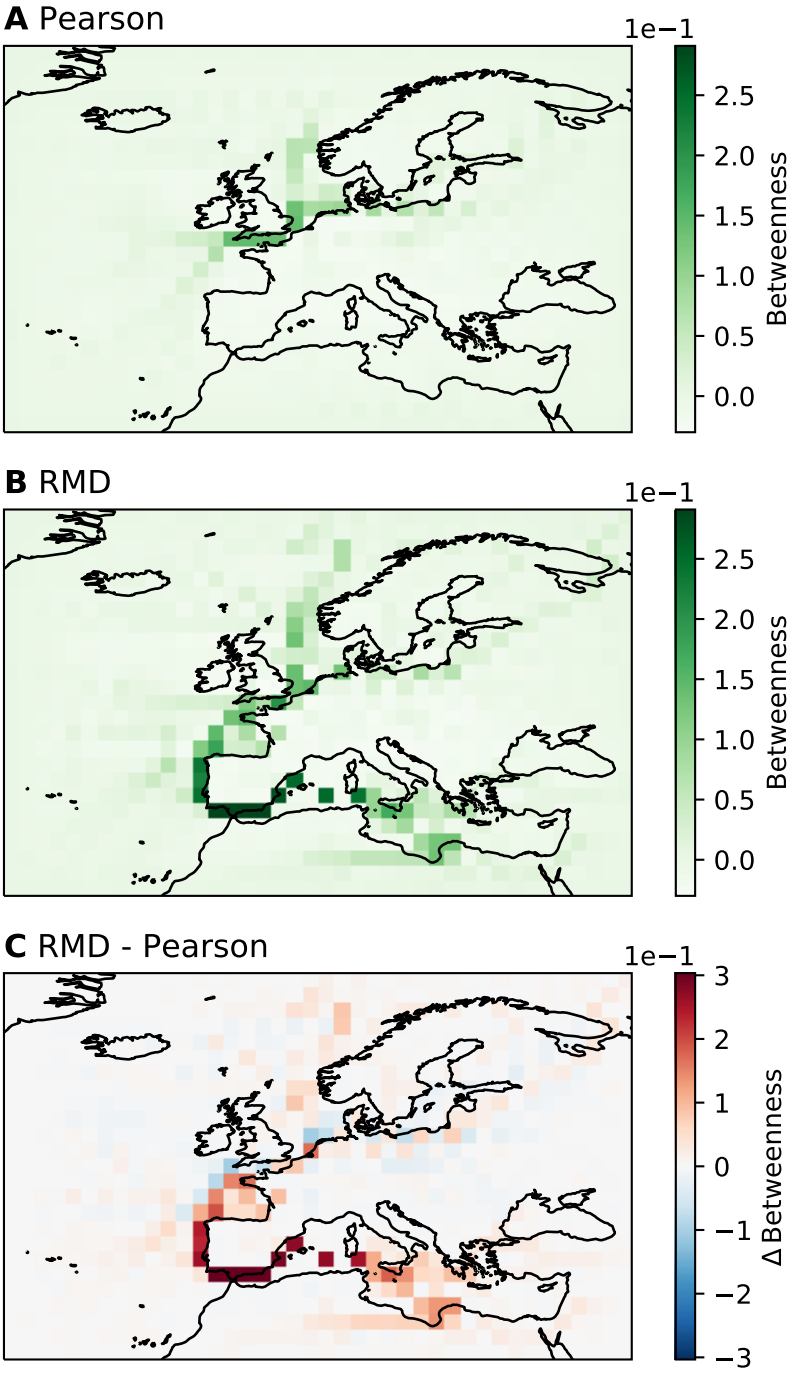

Figure 3. Betweenness fields for networks derived from Pearson correlation coefficient (**A**), recurrence based measure of dependence (RMD) (**B**) and their difference (**C**).

connected to other parts of the network. The hub west of Africa could be attributed to the Atlantic Oscillation, while the Mediterranean is known as a significant driver of European temperatures.

The RMD network however assigns higher AWC to nodes over France and Russia. This means that either the RMD missed linear correlations in Southern Europe or found stronger non-linear correlations that - due to the constrained link density - suppressed the linear correlations seen in the Pearson network. Another explanation could be that these features reflect the effect of climate change on winter temperatures. The high-degree area over Russia seen in the AWC plot coincides with the highest rate of warming in Europe. Why a RMD network would pick up the warming trend, but the Pearson network would not, remains unclear.

Regardless of this difference, both networks display a drop in AWC at coastlines, indicating that these regions are less integrated into the network. This could imply that temperature variability here depends mainly on local effects and not on other regions (Donges et al., 2009).

Interestingly, effects on the degree due to terrain can not be seen here but have been reported previously (Peron et al., 2014). I would have expected to see terrain-related features of the AWC field at least in the Alps.

3.3 Betweenness Field

The boundary-corrected betweenness field is shown in Fig. A.2. It is perhaps the most interesting result regarding the static network. Again, a clear difference between the Pearson and RMD network is visible, where the latter shows a line of high betweenness starting in the Norwegian sea, going through the English Channel, around the Iberian Peninsula and via the straight of Gibraltar into the Mediterranean. The Pearson network is mostly lacking this feature and only shows high betweenness in the English Channel.

According to Donges et al. (2009) these lines of high betweenness separate regions of highly interconnected nodes and are important pathways of information in the network. On the global scale they have for example been attributed to ocean circulations (Donges et al., 2009). Here, valid candidates could be the North Atlantic Current west of the British Isles and Norway and the Mediterranean Outflow. However, it is unclear why not all features of the former would be seen between Iceland and the British Isles and how the features in the English Channel or around the Iberian Peninsula can be explained.

The high betweenness in the Mediterranean could also be due to a separation between temperature dynamics in Northern Africa and Southern Europe. However, other climatological boundaries like the Alps are not seen but have a similar effect.

Perhaps the easiest explanation is simply based on the difference between ocean and continent. European temperatures depend significantly on conditions of the ocean. In the network this could be attributed by information flowing across the coastlines, resulting in high betweenness here. However, this approach would not explain the feature in the Mediterranean and why the betweenness is low for the African coast.

3.4 Evolving Network

Fig. 4A shows the daily mean temperature over Europe between 1980 and 2022. A clear linear trend due to climate change is visible. Even though I accumulated weekly winter temperatures for the analysis, the plot shows yearly averages between

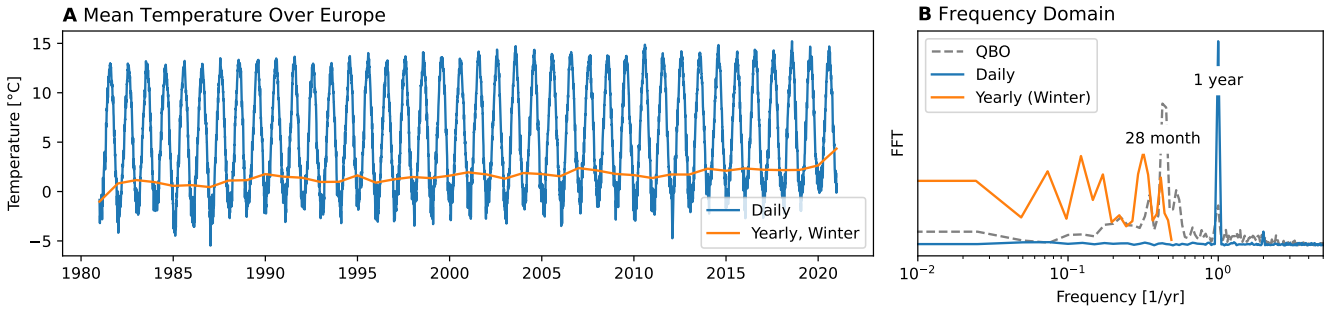

Figure 4. Daily time series of mean temperatures and yearly winter temperatures for Europe (**A**) and amplitudes of their frequency components (**B**). The Fourier spectrum of the QBO is equally shown and has a peak at $28\,\mathrm{month}$. The annual cycle is clearly visible in the daily series, however, neither daily nor yearly winter time series show a component at the QBO frequency.

October and March. This is because the evolving network analysis yields one network every year. On the right, in Fig. 4B, the frequency spectrum of both signals and the QBO index is shown. One can clearly see the annual cycle in the daily data and the QBO at 28 months respectively. However, yearly winter temperatures do not indicate any component at the QBO frequency. From the raw data alone, no effect of the QBO on European winter temperatures can thus be deduced.

Figures 5 and 6 show standardized metrics for the evolving networks derived from the Pearson correlation coefficient and the RMD. I used the global clustering coefficient, the average path length and the average closeness centrality. Additionally, the standardized QBO $70\,\mathrm{hPa}$ wind speed is shown for comparison. No network measure is really synchronous with the QBO. For the RMD network, some periods of synchronicity can be seen, however synchronization is unstable and breaks after a few cycles. This is also reflected in the frequency spectrum where a QBO component is visible but not larger than other frequency components. For the Pearson network the synchronization is even poorer.

Because the QBO is known to affect the Mediterranean region the strongest, I did a second analysis using only a subregion of the network (shown in Fig. A.1). However, results are equally poor and indicate no synchronicity with the QBO. Plots are nonetheless given in the Appendix.

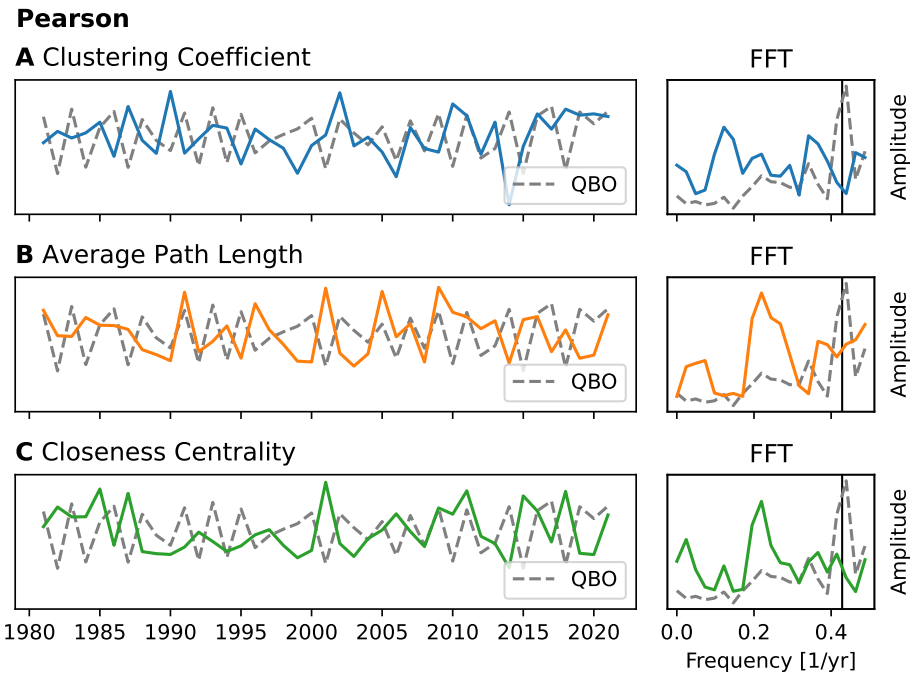

Figure 5. Standardized clustering coefficient (**A**), average path length (**B**) and closeness centrality (**C**) for the evolving Pearson network. The standardized QBO 70hPa wind speed is shown as the dashed line. On the right in the frequency domain, with the vertical bar indicating the mean QBO period.

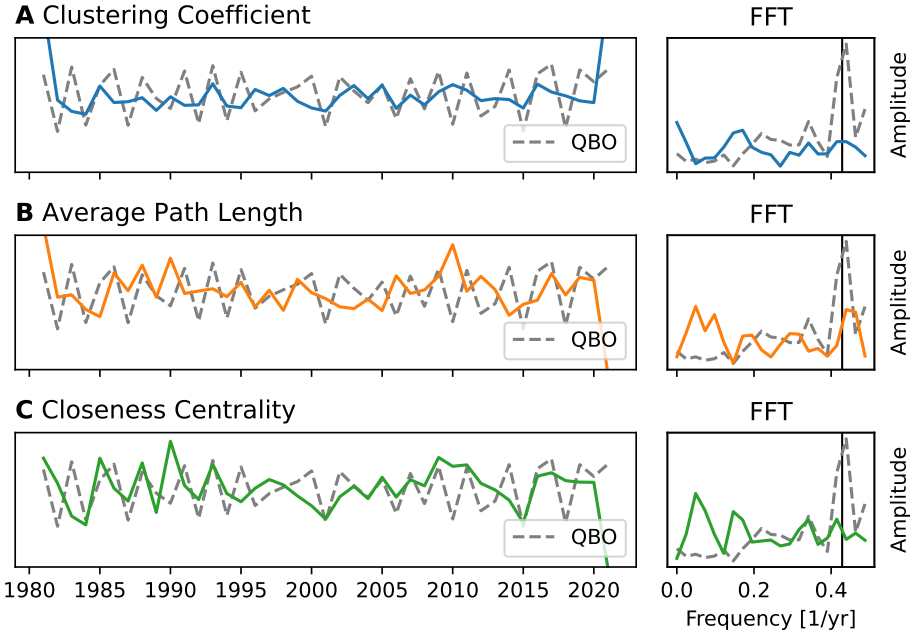

Figure 6. Standardized clustering coefficient (**A**), average path length (**B**) and closeness centrality (**C**) for the evolving RMD network. The standardized QBO 70hPa wind speed is shown as the dashed line. On the right in the frequency domain, with the vertical bar indicating the mean QBO period.

4 Discussion

4.1 Data Preparation

Firstly, the known linear trend in temperature could have been subtracted to remove the dominant effect of climate change. This was not done here. Both RMD and Pearson correlation are independent to linear transformations like scaling or shifting of the input data, but vary when a linear trend is added. However, the trend should affect all node pairs equally and thus not change the spatial patterns that are seen. I expect a simple rescaling of the Pearson and RMD correlation values that does not change their ordering and thus the links that are used in the network. Nonetheless, this was not verified and could contribute to the poor results when proven wrong.

Secondly, de-seasonalization should be done when not only winter temperatures are used. While this is done here by constraining the time series to winter months, a cleaner approach would be to use all available data but de-seasonalize it beforehand. This would not diminish effects by the QBO, as they happen with a different period.

4.2 Evolving Network Analysis

This study was not able to reliably pick up any influence of the QBO on European winter temperatures. I propose that this is due to a faulty methodological setup.

The temporal resolution of the evolving network analysis is one year. This limit was necessary because a higher sampling rate (seasonal or monthly) would require a daily and not weekly resolution in the time series, increasing the computational effort dramatically. However, I was interested in oscillations with a period of 28 months. The corresponding frequency of around $0.43\,\mathrm{yr}^{-1}$ is just smaller than the Nyquist frequency of $0.5\,\mathrm{yr}^{-1}$ that is associated with the used sampling rate. By the Shannon-Nyquist Sampling Theorem, the Nyquist frequency constitutes an upper limit to the frequency components that can be reliably observed in a discretized signal. When the criterion is not met, the signal is distorted in what is called the aliasing effect. Given the low number of samples (41) in combination with the operation close to the Nyquist frequency, it is reasonable to expect poor results. Furthermore, the problem is amplified because the QBO target frequency is unstable and can in principle exceed the Nyquist frequency at times.

To overcome this issue a higher sampling rate would be needed. Given sufficient computational power and time, at least seasonal windows with daily resolution would be beneficial, while monthly windows would be favorable. This would increase the Nyquist frequency fourfold to twelvefold. Additionally, apart from the computational benefit, there is no need to constrain the analysis to winter temperatures. Using all available data and constructing the evolving network for other seasons, too, would allow a more profound analysis of the QBO's effect on winter temperatures because a baseline for comparison would become available.

4.3 Other Network Metrics

I also looked at the spatially resolved clustering coefficient, closeness centrality and average path length, with plots of the former two shown in the Appendix. However, results are inconclusive and appear to be primarily due to artifacts. Why this is the case here but not for AWC and betweenness remains unclear. Unfortunately, the three problematic measures are also the ones employed to analyze the evolving network representation. This is simply due to the fact that for this analysis I needed measures that summarize the whole network in a scalar number and there are only so much available. I considered calculating the link robustness or sliding-window Hamming distance but considered them unusable because of the low sampling rate.

Nonetheless, the problematic use of the worst-performing spatial measures for the temporal analysis could of course contribute to the poor results seen here.

4.4 Ground-Truth Comparison

Complex network theory is a novel tool to analyze the climate system. Results should thus be interpreted carefully and are especially vulnerable to the confirmation bias. During this study I formulated some questions that go beyond its scope.

How could you generate baselines to which results could be compared? Here, this could be done by employing simulated data from a climate model that is known to not display the QBO. Alternatively, including the whole time series of temperatures would provide a better baseline for comparison between summer and winter. This question however is fundamental to the general method: without a null-hypothesis one is not really able to attribute patterns with certainty.

How would an effect even look like? This question has a lot to do with expert knowledge in the field of interest. Without a reliable comparison that surely exhibits a pattern, one can not be sure to have seen it. With the described methodological setup, the results are derived first and then interpreted. However, it is often better to hypothesize results and search for them and not stumble upon anything of interest in the process.

5 Conclusion

Based on gridded reanalysis data of European winter temperatures, this study has shown that both static and evolving complex climate networks can be constructed from a measure of dependence based on joint recurrences (RMD). Networks corrected for the boundary effect exhibit very similar properties overall when compared to ones created from the linear Pearson correlation. However, they differ strongly on the local scale. These overall similarities can be attributed to a similar construction scheme while local dissimilarities are mainly due to the visibility of non-linear effects in the RMD network.

To access a possible effect of the quasi-biennial oscillation (QBO) on European winter temperatures, this study used an evolving network representation. Time series of summarizing network measures like average clustering, path length and centrality do vary but indicate no oscillations synchronous with the QBO or abrupt transitions. This is true over the whole of Europe, as well as the Mediterranean that is known to be especially effected by the QBO. Certain periods of synchronicity can

be seen for the Pearson network but could also be attributed to the confirmation bias. An effect of the QBO on European winter temperatures could thus not be reliably detected.

This inability to detect the QBO was mainly attributed to a flaw in the methodological setup. The evolving network analysis was done with a period of one year, resulting in a Nyquist frequency that is very close to the targeted QBO oscillation of on average 28 months. Any visible signal is therefore rendered unreliable and confidence in the results is drastically reduced.

Code and data availability. All code and data is available on a dedicated GitHub repository: https://github.com/david-strahl/quasibi-europe.

References

Baldwin, M. P., Gray, L. J., Dunkerton, T. J., Hamilton, K., Haynes, P. H., Randel, W. J., Holton, J. R., Alexander, M. J., Hirota, I., Horinouchi, T., Jones, D. B., Kinnersley, J. S., Marquardt, C., Sato, K., and Takahashi, M.: The quasi-biennial oscillation, Reviews of Geophysics, 39, 179–229, https://doi.org/10.1029/1999RG000073, 2001.

Donges, J. F., Zou, Y., Marwan, N., and Kurths, J.: Complex networks in climate dynamics: Comparing linear and nonlinear network construction methods, European Physical Journal: Special Topics, 174, 157–179, https://doi.org/10.1140/epjst/e2009-01098-2, 2009.

Goswami, B., Marwan, N., Feulner, G., and Kurths, J.: How do global temperature drivers influence each other?: A network perspective using recurrences, European Physical Journal: Special Topics, 222, 861–873, https://doi.org/10.1140/epjst/e2013-01889-8, 2013.

Hagberg, A. A., Schult, D. A., and Swart, P. J.: Exploring Network Structure, Dynamics, and Function using NetworkX, in: Proceedings of the 7th Python in Science Conference, edited by Varoquaux, G., Vaught, T., and Millman, J., pp. 11 – 15, Pasadena, CA USA, 2008.

Peron, T. K., Comin, C. H., Amancio, D. R., Da, L., Rodrigues, F. A., and Kurths, J.: Correlations between climate network and relief data, Nonlinear Processes in Geophysics, 21, 1127–1132, https://doi.org/10.5194/npg-21-1127-2014, 2014.

Rheinwalt, A., Marwan, N., Kurths, J., Werner, P., and Gerstengarbe, F. W.: Boundary effects in network measures of spatially embedded networks, EPL, 100, https://doi.org/10.1209/0295-5075/100/28002, 2012.

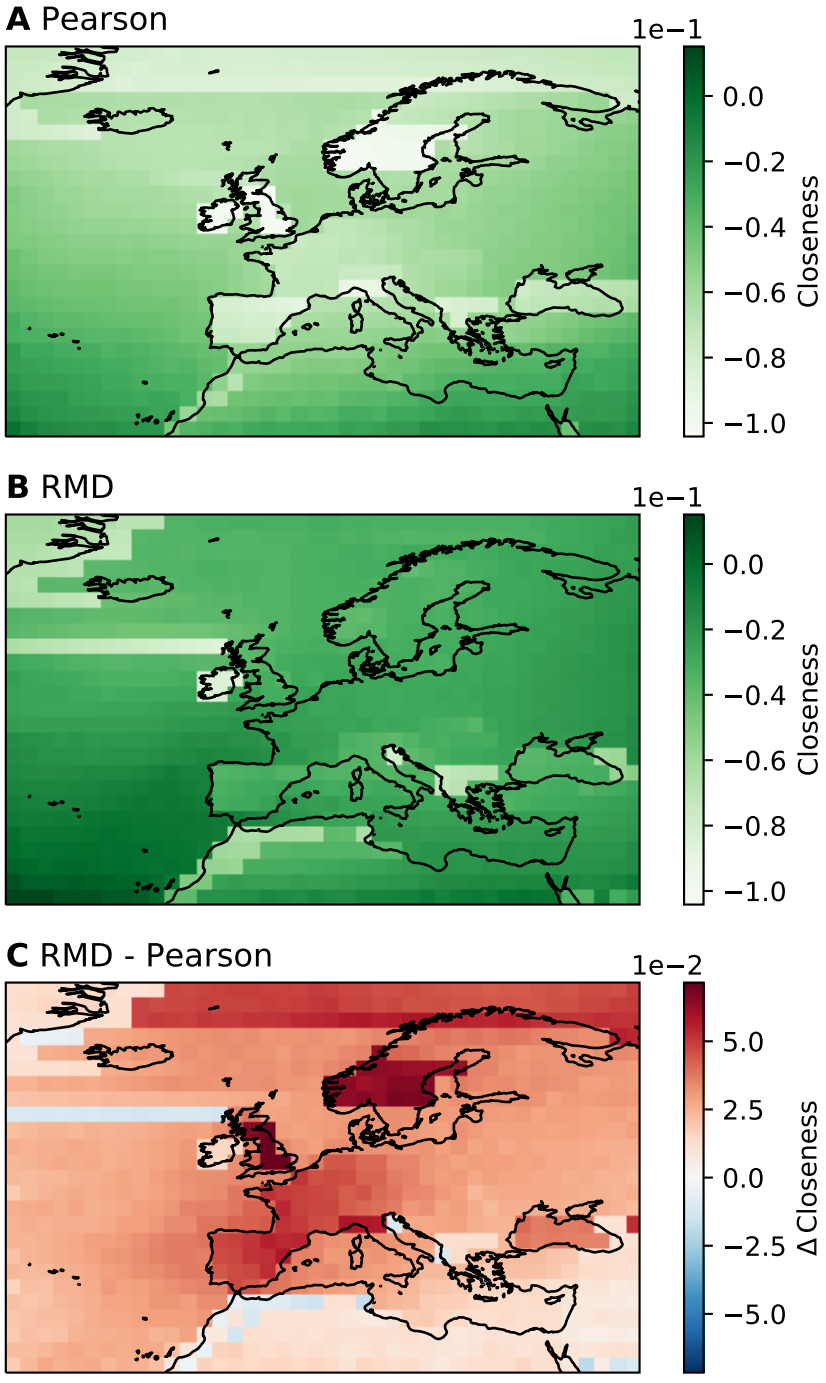

Figure A.1. Closeness fields for networks derived from Pearson correlation coefficient (**A**), recurrence based measure of dependence (RMD) (**B**) and their difference (**C**).

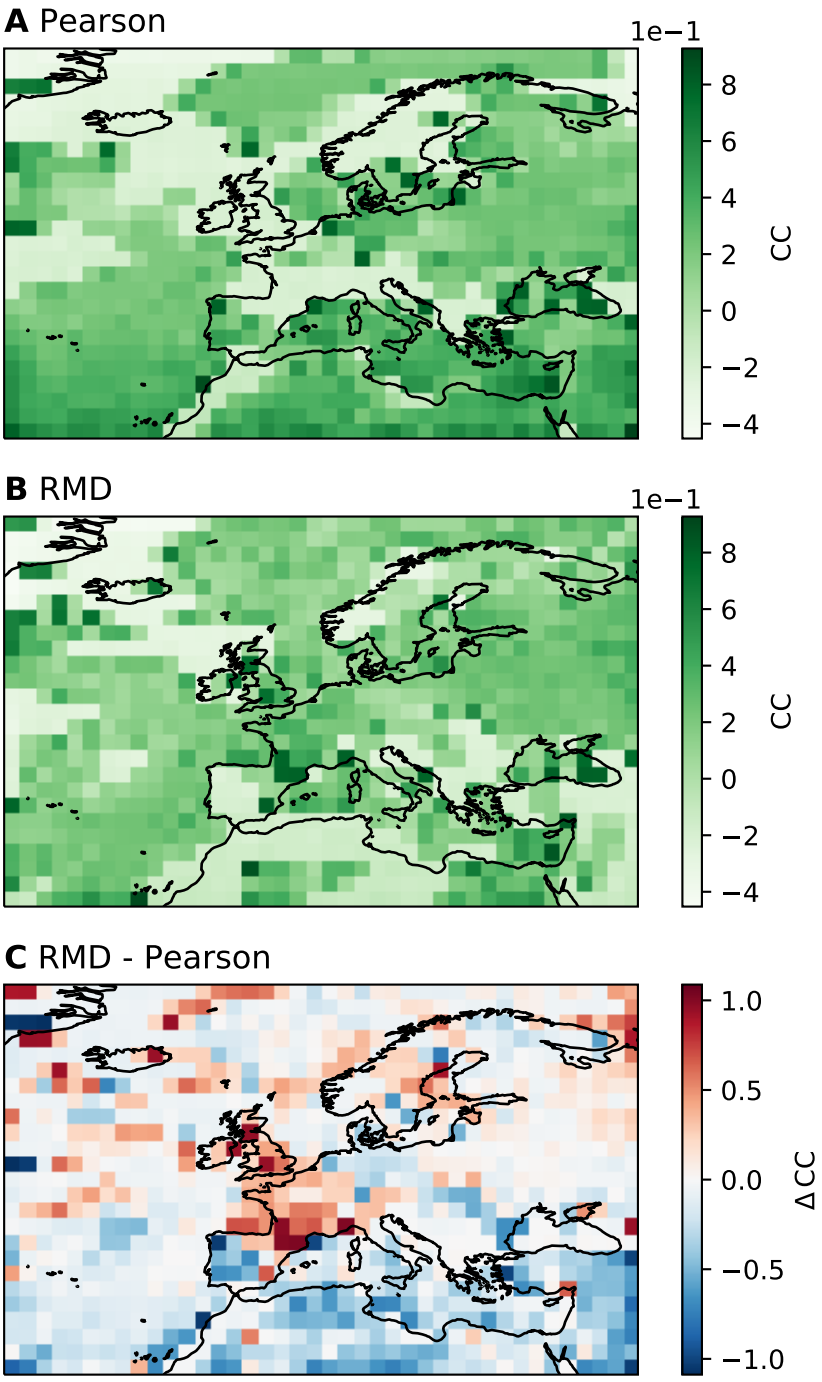

Figure A.2. Clustering coefficient fields for networks derived from Pearson correlation coefficient (**A**), recurrence based measure of dependence (RMD) (**B**) and their difference (**C**).

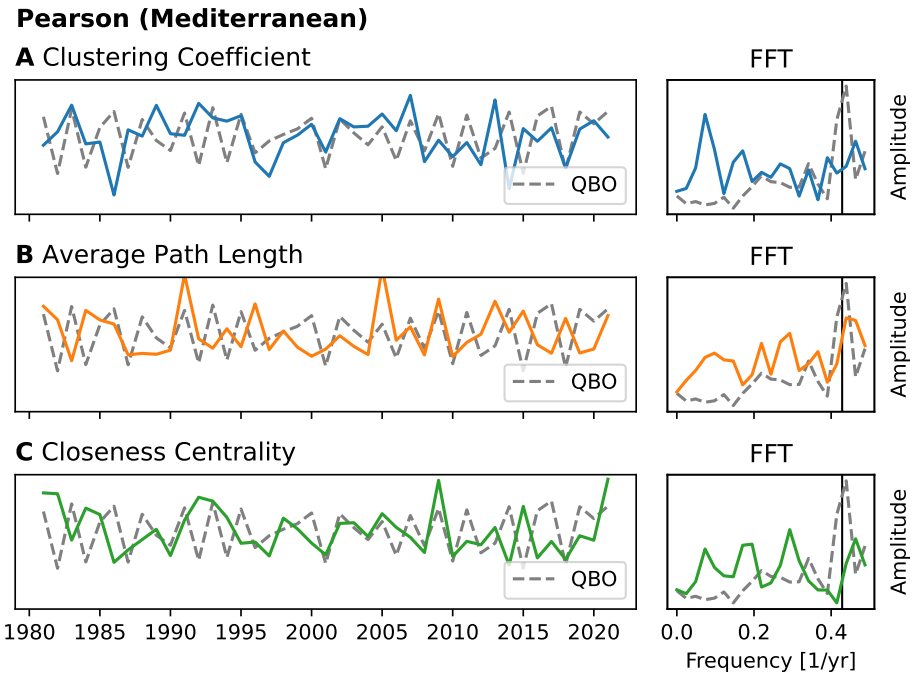

Figure A.3. Standardized clustering coefficient (**A**), average path length (**B**) and closeness centrality (**C**) for the evolving Pearson network over the Mediterranean. The standardized QBO 70hPa wind speed is shown as the dashed line. On the right in the frequency domain, with the vertical bar indicating the mean QBO period. Periods of rough synchronicity can be seen for all three network metrics.

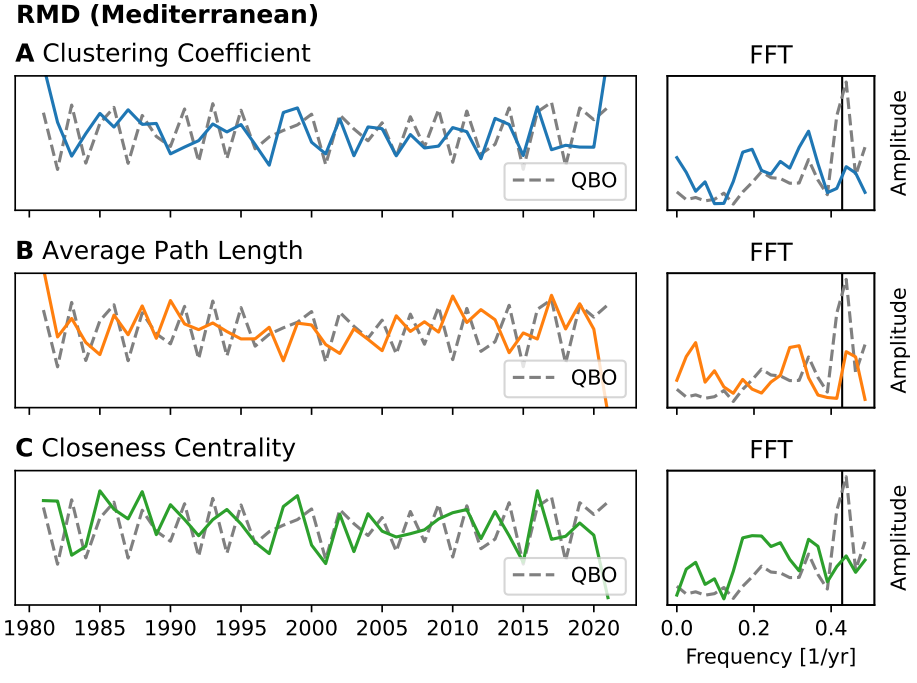

Figure A.4. Standardized clustering coefficient (**A**), average path length (**B**) and closeness centrality (**C**) for the evolving RMD network over the Mediterranean. The standardized QBO 70hPa wind speed is shown as the dashed line. On the right in the frequency domain, with the vertical bar indicating the mean QBO period. Metrics derived from evolving RMD networks show poorer synchronicity with the QBO.